Chemical Science

ROYAL SOCIETY OF CHEMISTRY

EDGE ARTICLE

View Article Online
View Journal | View Issue

Cite this: *Chem. Sci.*, 2024, **15**, 16612

All publication charges for this article have been paid for by the Royal Society of Chemistry

Received 31st May 2024
Accepted 12th September 2024

DOI: 10.1039/d4sc03571b

rsc.li/chemical-science

The H/F substitution strategy can achieve large spontaneous polarization in 1D hybrid perovskite ferroelectrics†

Jiu-Yang Liu,[a] Meng-Meng Lun,[a] Zhi-Jie Wang,[a] Jun-Yi Li,[a] Kun Ding,[a] Da-Wei Fu, *[a] Hai-Feng Lu *[b] and Yi Zhang *[b]

Hybrid organic–inorganic perovskite (HOIP) ferroelectrics exhibit polarization reversibility and have a wide range of applications in the fields of smart switches, memorizers, sensors, *etc.* However, the inherent limitations of small spontaneous polarization (P_s) and large coercive field (E_c) in ferroelectrics have impeded their broader utilization in electronics and data storage. Molecular ferroelectrics, as a powerful supplement to inorganic ferroelectrics, have shown great potential in the new generation of flexible wearable electronic devices. The important research responsibility is to greatly improve progressiveness and overcome the above limitations. Here, a novel one-dimensional (1D) HOIP ferroelectric, (3-F-BTAB)$PbBr_3$ (3-F-BTAB = 3-fluorobenzyltrimethylammonium), was successfully synthesized by employing the H/F substitution strategy to modify parent compound (BTAB)$PbBr_3$ (BTAB = benzyltrimethylammonium), which undergoes a ferroelectric phase transition with Aizu notation 2/*m*F2 at 420 K. Notably, (3-F-BTAB)$PbBr_3$ demonstrates exceptional ferroelectric properties with a large P_s of 7.18 μC cm^{-2} and a low E_c of 1.78 kV cm^{-1}. As far as we know, (3-F-BTAB)$PbBr_3$ features the largest P_s among those reported for 1D lead-based HOIP ferroelectrics. This work enriches the 1D lead-based ferroelectric family and provides guidance for applying ferroelectrics in low-voltage polar memories.

Introduction

Ferroelectrics with switchable spontaneous polarization under the applied electric field are widely used in the fields of data storage devices, transducers and sensors.[1–9] The main research on ferroelectrics has always been inorganic oxides, such as $BaTiO_3$ (BTO) and Pb(Zr, Ti)O_3 (PZT) for their large P_s and longitudinal piezoelectric coefficient (d_{33}) since the discovery of Rochelle salt (potassium sodium tartrate tetrahydrate).[10–12] Molecular ferroelectrics, as a powerful supplement to inorganic ceramic ferroelectrics, have shown great potential in the new generation of flexible wearable electronic devices. With the development of molecular ferroelectrics in the past decades, ferroelectrochemistry has been a hot topic in the interdisciplinary fields of physics, chemistry, information, and electronics,[13–17] which has led to the subsequent discovery of organic ferroelectrics such as diisopropylammonium bromide (DIPAB) with large P_s (23 μC cm^{-2}) and high Curie temperature (T_c = 426 K). DIPAB is the first molecular ferroelectric to rival BTO, and its discovery is a notable achievement in the advancement of molecular ferroelectrics.[18] The organic and inorganic components are able to self-assemble into HOIPs through weak intermolecular interactions, which have advantages of both organic cations and inorganic anions, exhibiting diverse structures, rich properties, and mechanical flexibility.[19–30] This structure serves as an ideal template for constructing ferroelectrics and facilitates the optimization of their properties by chemical modification strategies.[18,31–33] As we all know, P_s and E_c are two important parameters to characterize ferroelectricity. Optimizing the performance of ferroelectrics by increasing P_s and decreasing E_c has been a longstanding endeavor, aiming to apply them in the field of non-volatile memory and electronic devices with lower energy consumption and longer work lifespan.[34–37] Despite the extensive research that has been undertaken, the improvement of ferroelectricity for HOIPs is still confronted with challenges.

Fortunately, HOIPs exhibit rich structural modifiability and compositional flexibility, allowing for chemical modification strategies such as homochirality, quasi-spherical strategy and H/F substitution strategy.[38–43] Among them, the H/F substitution is regarded as an effective strategy to design ferroelectrics

[a]*Ordered Matter Science Research Center, Jiangsu Key Laboratory for Science and Applications of Molecular Ferroelectrics, Southeast University, Nanjing 211189, People's Republic of China. E-mail: dawei@seu.edu.cn*

[b]*Institute for Science and Applications of Molecular Ferroelectrics, Key Laboratory of the Ministry of Education for Advanced Catalysis Materials, Zhejiang Normal University, Jinhua 321019, People's Republic of China. E-mail: luhaifeng@zjnu.edu.cn; yizhang1980@seu.edu.cn*

† Electronic supplementary information (ESI) available: Experimental section, Fig. S1–S9 and Tables S1–S3. CCDC 2350277, 2350294–2350295. For ESI and crystallographic data in CIF or other electronic format see DOI: https://doi.org/10.1039/d4sc03571b

and optimize ferroelectric properties. Fluorine atoms exhibit higher electronegativity than hydrogen atoms, as well as they have analogous van der Waal's radii and steric hindrances, but substituting hydrogen atoms with fluorine atoms can regulate significantly the chemical and physical properties of materials. Compared to the isotope substitution only applicable to hydrogen-bonded molecular ferroelectrics, H/F substitution can increase the dipole moment, induce phase transitions, and improve the phase transition temperature, which has greater development space for the design and regulation of high-performance ferroelectrics.

Sha *et al.* synthesized the initial fluorinated 2D lead iodide perovskite ferroelectric $(DFCHA)_2PbI_4$ (DFCHA = 4, 4-difluorocyclohexylammonium) through the H/F substitution strategy, the P_s of which is estimated to be 4.5 μC cm^{-2} only according to the point charge model.[44] Additionally, Shi *et al.* methodically incorporated fluorine substituents into the organic cations of $[BA]_2PbCl_4$ (BA = benzylammonium), and acquired a novel HOIP ferroelectric $[2\text{-FBA}]_2PbCl_4$ (2-FBA = 2-fluorobenzylammonium) with a P_s of 5.35 μC cm^{-2} and an E_c of 15 kV cm^{-1}.[45] Although extensive research has been conducted based on the H/F substitution strategy, the issue of small P_s and high E_c remains. We still need to further explore the research and development of HOIP ferroelectrics with large P_s and low E_c for better commercial applications.

Here, we synthesized a 1D HOIP ferroelectric (3-F-BTAB)$PbBr_3$ through the H/F substitution strategy based on the parent (BTAB)$PbBr_3$ (Scheme 1). Compared to (BTAB)$PbBr_3$ crystallized in the centrosymmetric space group $C2/c$, the fluorinated (3-F-BTAB)$PbBr_3$ crystallizes in the non-centrosymmetric space group $C2$ and undergoes a ferroelectric phase transition (the Aizu notation $2/m$F2) at a high temperature of 420 K.[46] The measurement results of the ferroelectric hysteresis loop indicate that (3-F-BTAB)$PbBr_3$ can realize polarization reversal at room temperature when applied a small electric field (E_c = 1.78 kV cm^{-1}). In fact, as far as we know, the P_s of (3-F-BTAB)$PbBr_3$ is 7.18 μC cm^{-2} which is the highest among those reported for reported 1D organic–inorganic hybrid lead-based ferroelectrics.[40,47–49] Notably, (3-F-BTAB)$PbBr_3$ exhibits a high decomposition temperature and can also possess a long service life when below the T_c (T_c = 420 K), which is essential for the application of ferroelectric-related electronic components. In addition to ferroelectricity, (3-F-BTAB)$PbBr_3$ reveals excellent nonlinear optical, photoluminescence and semiconductor properties. This work sheds light on exploring more high-performance 1D lead-based HOIP ferroelectrics for application in low-voltage memories.

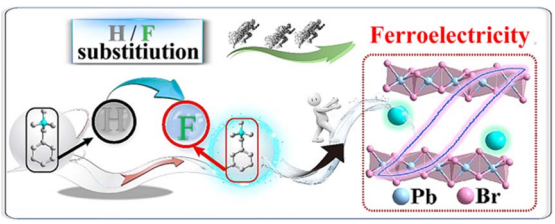

Scheme 1 Design strategy for obtaining organic–inorganic hybrid ferroelectrics.

Results and discussion

Thermal properties and dielectric properties

The colorless transparent single crystal of (3-F-BTAB)$PbBr_3$ in a size of 2 × 2 × 7 mm^3 was prepared by solvent volatilization (Fig. 1b), and powder X-ray diffraction (PXRD) was used to verify its phase purity (Fig. S1†). Differential scanning calorimetry (DSC) is a commonly employed thermal analysis method, which can determine the existence of phase transition behavior by studying the heat change of a substance with temperature. DSC curves of (BTAB)$PbBr_3$ and (3-F-BTAB)$PbBr_3$ are shown in Fig. S2† and 1a. For (BTAB)$PbBr_3$, there are no obvious thermal anomalies within the temperature range of 260–420 K, suggesting that no phase transition behavior occurred in (BTAB)$PbBr_3$ throughout the examined temperature range. However, for (3-F-BTAB)$PbBr_3$, its DSC curves show a pair of significant endothermic and exothermic peaks at 420 and 412 K, respectively. According to the DSC curves of (3-F-BTAB)$PbBr_3$, the entropy change ΔS is determined to be 2.08 J mol^{-1} K^{-1} by the formula $\Delta S = \Delta H/T$ (ΔH = 873.6 J mol^{-1}). For simplicity, the structure of (3-F-BTAB)$PbBr_3$ when the temperature is above T_c is regarded as the high-temperature phase (HTP), and below T_c is regarded as the low-temperature phase (LTP). The results show that the H/F substitution strategy successfully induced the phase transition behavior of (3-F-BTAB)$PbBr_3$, which possesses high phase transition temperature and small thermal hysteresis. For solid–solid phase transition materials, their dielectric constants usually exhibit significant anomalies at their phase transition temperatures and show temperature and frequency dependency. As shown in Fig. 1c and S3†, the dielectric constant slowly increases with the increase of temperature below the phase transition temperature and a λ-shaped dielectric peak appears near 420 K, which is in accordance with the DSC

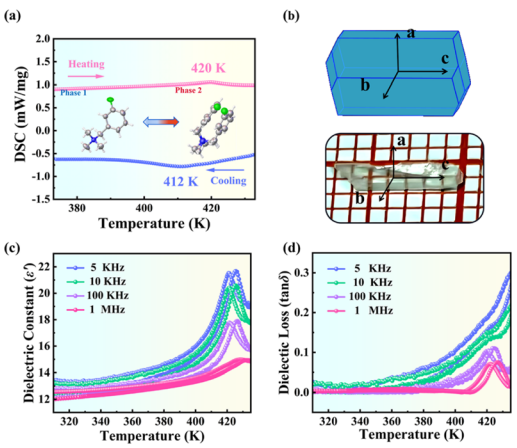

Fig. 1 (a) DSC curves of (3-F-BTAB)$PbBr_3$ in the heating–cooling cycle. (b) The image and simulated crystal growth morphology of the crystal. (c) Temperature dependence of the real part (ε') of (3-F-BTAB)$PbBr_3$ at different frequencies. (d) Dielectric loss (tan δ) of (3-F-BTAB)$PbBr_3$ as a function of temperature.

measurements. The dielectric loss (tan δ) of (3-F-BTAB)$PbBr_3$ as a function of temperature is shown in Fig. 1d. In addition, the Curie–Weiss law fits the dielectric response well, indicating the presence of a ferroelectric phase transition. Based on the formula $\varepsilon' = C_{para}/(T - T_0)$ for the paraelectric phase, or $\varepsilon' = C_{ferro}/(T_0' - T)$ for the ferroelectric phase (C_{para} and C_{ferro} represent the Curie constants, $T_0'$and T_0 represent the Curie–Weiss temperatures for the ferroelectric and paraelectric phases, respectively). C_{para} and C_{ferro} are calculated to be approximately 10 482 and 3676 K respectively at 1 MHz (Fig. S4†). The C_{para}/C_{ferro} ratio of (3-F-BTAB)$PbBr_3$ is 2.85 at 1 MHz, which tends to be a second-order ferroelectric transition around 420 K.[50]

Crystallographic structure analysis

In order to elucidate the mechanism of the reversible phase transition, the crystal structures of (BTAB)$PbBr_3$ and (3-F-BTAB)$PbBr_3$ were determined using single crystal X-ray diffraction (SC-XRD). As shown in Table S1† the parent (BTAB)$PbBr_3$ crystallizes at room temperature in the monoclinic space group $C2/c$ (point group $2/m$), with cell parameters a = 23.110(3) Å, b = 9.6090(13) Å, c = 26.851(4) Å, β = 106.990(14)°, V = 5702.4(13) Å^3. Interestingly, the fluorinated (3-F-BTAB)$PbBr_3$ crystallizes at LTP in the monoclinic non-centrosymmetric space group $C2$ (point group 2), with cell parameters a_{LTP} = 23.977(5) Å, b_{LTP} = 8.9117(16) Å, c_{LTP} = 7.7036(15) Å, β_{LTP} = 101.973(5)°, V_{LTP} = 1610.3(5) Å^3 (Table S1†). The organic cations and inorganic anions form the 1D ABX_3 perovskite structure through intermolecular interactions (Fig. 2a and b). The inorganic components are composed of face-shared octahedral $[PbBr_3]^-$ infinite chains (Fig. S5†), with Br–Pb–Br bond angles ranging from 81.59(2)° to 100.24(4)° and bond lengths ranging from 2.9080(10) Å to 3.1875(10) Å (Table S2†), respectively. To better illustrate the arrangement of the compound, the inorganic skeleton and the organic part are separately drawn. In LTP, the dipoles of the whole composed of inorganic and organic parts are along the b-axis. However, in HTP, the dipoles of inorganic and organic parts cancel out (Fig. 2c and d). As shown in Fig. 3a, from the polarization perspective, the centers of positive and negative charges do not coincide along the b direction, such an arrangement should lead to spontaneous polarization along the b-axis. In HTP, (3-F-BTAB)$PbBr_3$ crystallizes in the centrosymmetric space group $C2/c$, with cell parameters a_{HTP} = 23.5064(18) Å, b_{HTP} = 8.9668(5) Å, c_{HTP} = 6.8118(4) Å, β_{HTP} = 98.299(7)°, V_{HTP} = 1420.74(16) Å^3. Due to the increase temperature, the vibration of the organic cation and inorganic anion frameworks becomes intense, accompanied by an ordered state to a disordered state (Fig. 3c and d). Therefore, the phase transition is driven by the order–disorder transition of both the organic cation and the inorganic anionic framework. The symmetric position of cations becomes a special position on the symmetry plane perpendicular to the b-axis, and the dipole moments along the b-axis cancel each other out, resulting in the disappearance of spontaneous polarization (Fig. 3b). According to the phase transition of compound from $2/m$ (HTP) to 2 (LTP) point group, the symmetry elements are reduced from four (E, C_2, σ_h, i) to two (E, C_2), belonging to the ferroelectric phase transition characterized by the Aizu notation of $2/m$F2 (Fig. 3e). Through comparison, it was found that the distance between the inorganic skeletons of (BTAB)$PbBr_3$ (15.9899(20) Å) is greater than that of (3-F-BTAB)$PbBr_3$ (12.7898(24) Å), so the

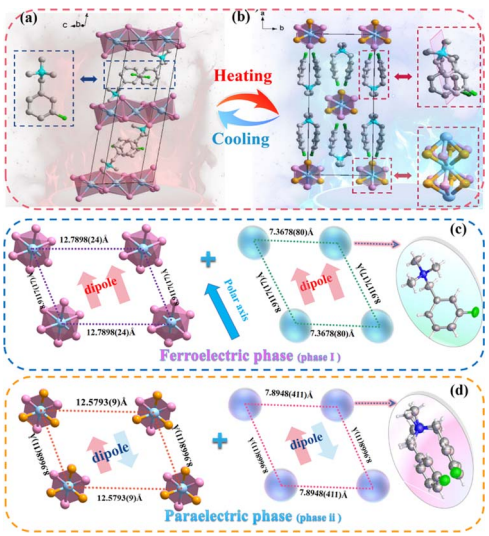

Fig. 2 Comparison of crystal structures of (3-F-BTAB)$PbBr_3$ in the LTP and HTP. (a) Packing view in the LTP. The $[3\text{-F-BTAB}]^+$ cations and $[PbBr_3]^-$ frameworks are ordered. (b) Packing view in the HTP. Both the $[3\text{-F-BTAB}]^+$ cations and $[PbBr_3]^-$ frameworks become disordered. The distance between adjacent inorganic frameworks along the b-axis and the distance between adjacent cations in the LTP (c) and HTP (d). H atoms were omitted for clarity.

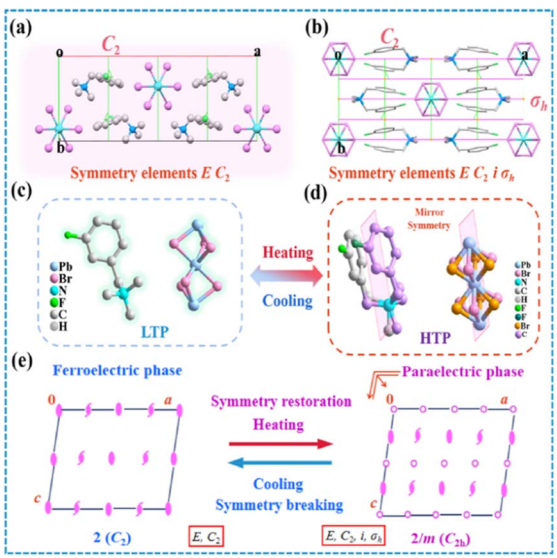

Fig. 3 Comparison of packing views of (3-F-BTAB)$PbBr_3$ at (a) LTP and (b) HTP along the c-axis. The $[3\text{-F-BTAB}]^+$ cations occupy a general symmetry position at LTP, yet a special position of the symmetry plane at HTP. (c) Molecular structure of (3-F-BTAB)$PbBr_3$ crystallized as the low temperature phase. (d) Molecular structure of (3-F-BTAB)$PbBr_3$ crystallized as the high temperature phase, the pink planes are mirrors only existing in the high temperature phase. (e) Symmetry breaking occurs with an Aizu notation of $2/m$F2 in (3-F-BTAB)$PbBr_3$.

arrangement of organic cations and inorganic skeletons of (3-F-BTAB)$PbBr_3$ is more compact. In addition, there are intermolecular interactions between the H and F atoms of adjacent cations, as well as between the H atom on the cation and the inorganic skeleton in (3-F-BTAB)$PbBr_3$, compared to (BTAB)$PbBr_3$ (Fig. S8 and S9†). A new polar substance was obtained by precise molecular modification and design of non-polar substances, and it is exciting that this work will be a greater space to enrich the molecular ferroelectric family with the H/F substitution strategy in the future.

Second harmonic generation (SHG) and ferroelectricity

Generally, the second harmonic generation (SHG) response only exists in non-centrosymmetric crystals (except for point groups 422, 622 and 432) and is a common method for characterizing structural symmetry and verifying phase transition behavior. The intense SHG signal (1.5 KDP) of (3-F-BTAB)$PbBr_3$ can be observed at room temperature, consistent with the non-centrosymmetric $C2$ space group (Fig. 4a). To further verify the phase transition of (3-F-BTAB)$PbBr_3$ from non-centrosymmetric $C2$ to centrosymmetric $C2/c$, we measured the variation of SHG response with temperature (Fig. 4b). At 300–405 K, the SHG intensity is approximately 1.5 times that of KH_2PO_4 (KDP), presenting a high SHG signal response. The SHG intensity undergoes a sudden change near the phase transition temperature and the signal intensity sharply decreases to nearly 0, indicating a low SHG response. The reversible step-like response between LTP and HTP was observed during the heating–cooling cycle, in accordance with the symmetry requirements from the polar ferroelectric phase to the centrosymmetric paraelectric phase, indicating that (3-F-BTAB)$PbBr_3$ is a potential nonlinear optical switching material. Combined with notable variations in dielectric anomalies, the ferroelectricity of (3-F-BTAB)$PbBr_3$ necessitates additional validation through the measurement of the polarization–electric field (P–E) hysteresis loop.[51] As shown in Fig. 4c, the P–E loop exhibits a characteristic rectangular shape, providing confirmation of the ferroelectricity of (3-F-BTAB)$PbBr_3$. When the frequency is 50 Hz, the result shows that the E_c and P_s of (3-F-BTAB)$PbBr_3$ are 1.78 kV cm^{-1} and 7.18 μC cm^{-2} at room temperature, respectively, which indicates that the ferroelectric can undergo polarization reversal even with a rather low E_c. To our knowledge, the P_s is currently the highest among those reported for 1D lead-based HOIP ferroelectrics (Fig. 4f). Following the experimental validation of ferroelectricity, we carried out ferroelectric polarization calculations utilizing the Berry phase method to understand its ferroelectricity further. Based on the crystal structures of (3-F-BTAB)$PbBr_3$ in LTP and HTP, we constructed a series of transition states (Fig. 4d). The dynamic evaluation path from the ferroelectric phase to the paraelectric phase is essential for estimating the theoretical polarization value. Through rotation and displacement of (3-F-BTAB)$PbBr_3$ to estimate reasonably, the results show that there is not much difference between the theoretical macroscopic polarization value ($P_s = 10.66$ μC cm^{-2}) and the measurement value (Fig. 4e).

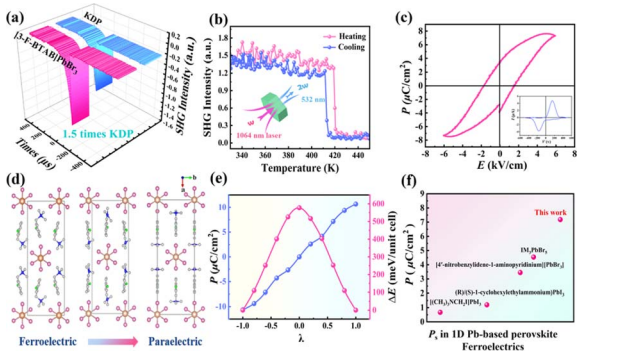

Fig. 4 (a) SHG intensity of (3-F-BTAB)$PbBr_3$ and KDP. (b) Temperature-dependent SHG response. (c) Polarization–electric field (P–E) hysteresis loop and I–V curve at 298 K by the Sawyer–Tower method. (d) Berry phase calculation of polarization from ferroelectric phase structures to constructed paraelectric phase structures of (3-F-BTAB)$PbBr_3$. (e) Calculated macroscopic polarization and attributions and changes of energy (ΔE) from diverse cations. (f) Comparison of P_s with those reported for 1D organic–inorganic hybrid lead-based ferroelectrics.

Photoluminescence properties

The 1D lead-based HOIPs generally exhibit optoelectronic properties. In this work, the photoluminescence (PL) characteristics of (3-F-BTAB)$PbBr_3$ are also studied. The compound shows strong orange luminescence under ultraviolet (UV) lamps of 254 and 365 nm (Fig. 5a), which is in accordance with the orange chromaticity coordinates as determined by the Commission Internationale de l'Eclairage (CIE) coordination (Fig. 5d). Under the excitation of 300 or 340 nm, obvious broadband emission peaks with the same intensity at 650 nm were observed (Fig. 5b). (3-F-BTAB)$PbBr_3$ has broadband emission and a large Stokes shift, which may be due to self-trapping excitons (STE) formed by the strong electron–phonon coupling of 1D octahedral chains.[52] The PL decay curve at 650 nm was measured using an excitation wavelength of 340 nm and the PL decay lifetime was 61.91 ns (Fig. S6†). According to the

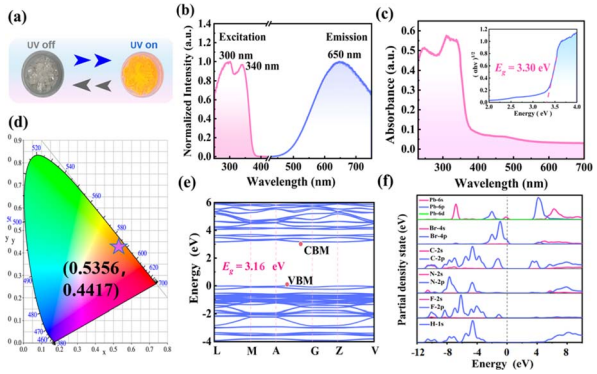

Fig. 5 (a) Crystal under ambient light and UV light irradiation at room temperature. (b) Normalized excitation and emission spectra of (3-F-BTAB)$PbBr_3$ at room temperature. (c) UV-visible absorption of (3-F-BTAB)$PbBr_3$ and optical band gaps were calculated using the Tauc equation. (d) CIE chromaticity coordinates (e) Band structure of (3-F-BTAB)$PbBr_3$. (f) Partial density of states (PDOS) of (3-F-BTAB)$PbBr_3$.

measured results, the photoluminescence quantum yield of (3-F-BTAB)$PbBr_3$ is 3.12% (Fig. S7†).

Semiconductor properties

Hybrid lead halide materials are potential semiconductor materials. To further understand the semiconductor properties of (3-F-BTAB)$PbBr_3$, UV-visible absorption spectroscopy and theoretical calculations were conducted to study the band structure. From the UV-absorption spectrum, it can be observed that there is strong absorption at the band of 320 nm, which is consistent with the characteristics of indirect semiconductors. Meanwhile, according to the Tauc equation $(\alpha h\nu)^{1/n} = A(h\nu - E_g)$, the optical bandgap of (3-F-BTAB)$PbBr_3$ is calculated to be 3.30 eV (Fig. 5c). The band structure and partial density of states (PDOS) of (3-F-BTAB)$PbBr_3$ were computed utilizing density functional theory (DFT) and the theoretical bandgap of (3-F-BTAB)$PbBr_3$ is 3.16 eV, close to the experimental bandgap (Fig. 5e). The conduction band minimum (CBM) and valence band maximum (VBM) values are situated at different positions in the Brillouin zone, so (3-F-BTAB) $PbBr_3$ belongs to an indirect bandgap semiconductor. According to the data of PDOS, the VBM is occupied by the electronic states of Br 4p, while the CBM is contributed by the Pb 6s state (Fig. 5f), so the bandgap of (3-F-BTAB)$PbBr_3$ is mainly contributed by the inorganic frameworks.

Conclusions

In summary, we successfully synthesized a novel 1D HOIP ferroelectric (3-F-BTAB)$PbBr_3$, with high performance through the implementation of the H/F substitution strategy. Compared with other harsh conditions requiring high temperature and pressure, (3-F-BTAB)$PbBr_3$ demonstrates the capability to reverse polarization at a low E_c (1.78 kV cm^{-1}) at ambient temperature, while also displaying a notably large P_s of 7.18 μC cm^{-2}. To our knowledge, this is the highest P_s reported for 1D HOIP lead-based ferroelectrics. Moreover, (3-F-BTAB)$PbBr_3$ exhibits remarkable nonlinear optical properties (signal intensity is up to 1.5 times KDP), photoluminescence, semiconductor properties and high Curie temperature (420 K), making it a high-performance ferroelectric. As a result, the precise molecular design the through H/F substitution strategy provides a novel perspective for future research on the synthesis of high-performance HOIP ferroelectrics.

Experimental

Synthesis and growth of crystals

All chemical reagents used in this work were obtained from commercial sources without further purification. The synthesis of the ligands BTAB and 3-F-BTAB can be referred to previous reports. 2 mmol of BTAB was weighed in a beaker and dissolved with hydrobromic acid, and then 2 mmol of $PbBr_2$ was added. After complete dissolution, the solution was slowly evaporated at room temperature, and after a few weeks, a colorless block crystal of (BTAB)$PbBr_3$ was obtained. The crystal of (3-F-BTAB) $PbBr_3$ was obtained in the same way.

Characterization

Measurement methods for Single-crystal X-ray Diffraction (SXRD), dielectric measurement, Differential Scanning Calorimetry (DSC), Powder XRD (PXRD), ferroelectric measurement and Second Harmonic Generation (SHG) are described in detail in the ESI†. Density functional theory (DFT) calculation methods and data are also shown in the ESI†.

Data availability

CCDC 2350277, 2350294–2350295 contain the supplementary crystallographic data for this paper.

Author contributions

J.-Y. L. conceived the experiments and wrote the paper. M.-M. L. and J.-Y. L. performed theoretical calculations. Z.-J. W. and K. D. assisted in the auxiliary analysis of data. D.-W. F., H.-F. L. and Y. Z. guided and supervised this work.

Conflicts of interest

The authors declare no conflict of interest.

Acknowledgements

This work was financially supported by the National Natural Science Foundation of China (grant 21991141, 22371258 and 22375182) and the research fund of Southeast University. We thank the Big Data Computing Center of Southeast University for providing the facility support on the numerical calculations in this paper.

Notes and references

1 H. Y. Zhang, Y. Y. Tang, Z. X. Gu, P. Wang, X. G. Chen, H. P. Lv, P. F. Li, Q. Jiang, N. Gu, S. Ren and R. G. Xiong, *Science*, 2024, **383**, 1492–1498.
2 Q. Q. Jia, H. F. Lu, J. Q. Luo, Y. Y. Zhang, H. F. Ni, F. W. Zhang, J. Wang, D. W. Fu, C. F. Wang and Y. Zhang, *Small*, 2024, **20**, e2306989.
3 Z. X. Zhang, H. Wang, H. F. Ni, N. Wang, C. F. Wang, P. Z. Huang, Q. Q. Jia, G. Teri, D. W. Fu, Y. Zhang, Z. An and Y. Zhang, *Angew. Chem., Int. Ed.*, 2024, **63**, e202319650.
4 K. Ding, H. Ye, C. Su, Y.-A. Xiong, G. Du, Y.-M. You, Z.-X. Zhang, S. Dong, Y. Zhang and D.-W. Fu, *Nat. Commun.*, 2023, **14**, 2863.
5 J.-Y. Li, T. Zhang, M.-M. Lun, Y. Zhang, L.-Z. Chen and D.-W. Fu, *Small*, 2023, **19**, 2301364.
6 T. Zhang, K. Xu, J. Li, L. He, D. W. Fu, Q. Ye and R. G. Xiong, *Natl. Sci. Rev.*, 2023, **10**, nwac240.
7 H.-F. Ni, L.-K. Ye, P.-C. Zhuge, B.-L. Hu, J.-R. Lou, C.-Y. Su, Z.-X. Zhang, L.-Y. Xie, D.-W. Fu and Y. Zhang, *Chem. Sci.*, 2023, **14**, 1781–1786.
8 H. Peng, J.-C. Qi, X.-J. Song, R.-G. Xiong and W.-Q. Liao, *Chem. Sci.*, 2022, **13**, 4936–4943.

9 Q.-Q. Jia, G. Teri, J.-Q. Luo, H.-F. Ni, P.-Z. Huang, M.-M. Lun, Z.-X. Zhang, Y. Zhang and D.-W. Fu, *J. Am. Chem. Soc.*, 2024, **146**, 21120–21128.
10 R. Clarke and A. M. Glazer, *Ferroelectrics*, 1976, **14**, 695–697.
11 J. Valasek, *Phys. Rev.*, 1921, **17**, 475–481.
12 Z. Zhao, V. Buscaglia, M. Viviani, M. T. Buscaglia, L. Mitoseriu, A. Testino, M. Nygren, M. Johnsson and P. Nanni, *Phys. Rev. B: Condens. Matter Mater. Phys.*, 2004, **70**, 024107.
13 Y. Ai, W. Q. Liao, Y. R. Weng, H. P. Lv, X. G. Chen, X. J. Song, P. F. Li and R. G. Xiong, *J. Am. Chem. Soc.*, 2023, **145**, 23292–23299.
14 Z. J. Feng, Y. A. Xiong, W. C. Sun, T. T. Sha, J. Yao, Q. Pan, H. Hu, S. Dong, R. G. Xiong and Y. M. You, *Adv. Mater.*, 2024, **36**, e2307518.
15 H. H. Jiang, X. J. Song, H. P. Lv, X. G. Chen, R. G. Xiong and H. Y. Zhang, *Adv. Mater.*, 2024, **36**, e2307936.
16 Y. Du, W. Q. Liao, Y. Li, C. R. Huang, T. Gan, X. G. Chen, H. P. Lv, X. J. Song, R. G. Xiong and Z. X. Wang, *Angew. Chem., Int. Ed.*, 2023, **62**, e202315189.
17 N. Zhang, W. Sun, Y. Zhang, H. H. Jiang, R. G. Xiong, S. Dong and H. Y. Zhang, *Nat. Commun.*, 2023, **14**, 5854.
18 D. W. Fu, H. L. Cai, Y. Liu, Q. Ye, W. Zhang, Y. Zhang, X. Y. Chen, G. Giovannetti, M. Capone, J. Li and R. G. Xiong, *Science*, 2013, **339**, 425–428.
19 M. M. Lun, C. Y. Su, Q. Q. Jia, Z. X. Zhang, J. Li, H. F. Lu, Y. Zhang and D. W. Fu, *Inorg. Chem. Front.*, 2023, **10**, 5026–5034.
20 J. Q. Luo, Q. Q. Jia, G. Teri, M. M. Lun, Z. J. Wang, Z. X. Zhang, Y. Zhang and D. W. Fu, *ACS Mater. Lett.*, 2023, **6**, 452–460.
21 Q. F. Luo, H. F. Ni, P. Z. Huang, M. Zhu, C. F. Wang, Q. H. Zhuo, D. W. Fu, Y. Zhang and Z. X. Zhang, *Mater. Chem. Front.*, 2023, **7**, 6247–6253.
22 J. Q. Luo, M. M. Lun, Q. Q. Jia, Z. J. Wang, H. F. Lu, Y. Zhang and D. W. Fu, *Chin. J. Chem.*, 2024, **42**, 1706–1712.
23 X.-T. Sun, H.-F. Ni, Y. Zhang and D.-W. Fu, *Chin. J. Struct. Chem.*, 2024, **43**, 100212.
24 B.-W. Deng, Z.-P. Rao, M.-J. Shen, K.-W. Liang, Y. Zhu, Z.-J. Wang, K. Ding, C.-Y. Su, M.-M. Lun, Z.-X. Zhang, Y. Zhang and D.-W. Fu, *J. Mater. Chem. C*, 2024, **12**, 6098–6105.
25 Y. Yu Zhang, J.-Q. Luo, Y. Han, W.-Y. Zhang, Y. Zhang, H.-F. Lu and D.-W. Fu, *Chin. Chem. Lett.*, 2024, DOI: 10.1016/j.cclet.2024.109530.
26 Z.-J. Wang, M.-J. Shen, Z.-P. Rao, P.-Z. Huang, M.-M. Lun, B.-W. Deng, J.-Y. Li, C.-F. Wang, H.-F. Lu, D.-W. Fu and Y. Zhang, *Inorg. Chem. Front.*, 2024, **11**, 2290–2299.
27 M.-M. Lun, H.-F. Ni, Z.-X. Zhang, J.-Y. Li, Q.-Q. Jia, Y. Zhang, Y. Zhang and D.-W. Fu, *Angew. Chem., Int. Ed.*, 2024, **136**, e202313590.
28 M.-M. Lun, J.-Q. Luo, Z.-X. Zhang, J. Li, L.-Y. Xie, H.-F. Lu, Y. Zhang and D.-W. Fu, *Chem. Eng. J.*, 2023, **475**, 145969.
29 M.-M. Lun, C.-Y. Su, J. Li, Q.-Q. Jia, H.-F. Lu, D.-W. Fu, Y. Zhang and Z.-X. Zhang, *Small*, 2023, **19**, 2303127.
30 Z.-J. Wang, H.-F. Ni, T. Zhang, J. Li, M.-M. Lun, D.-W. Fu, Z.-X. Zhang and Y. Zhang, *Chem. Sci.*, 2023, **14**, 9041–9047.
31 H.-F. Ni, J.-H. Lin, G. Teri, Q.-Q. Jia, P.-Z. Huang, H.-F. Lu, C.-F. Wang, Z.-X. Zhang, D.-W. Fu and Y. Zhang, *Chin. Chem. Lett.*, 2024, DOI: 10.1016/j.cclet.2024.109690.
32 D. W. Fu, J. X. Gao, W. H. He, X. Q. Huang, Y. H. Liu and Y. Ai, *Angew. Chem., Int. Ed.*, 2020, **59**, 17477–17481.
33 Y. Zhang, X. J. Song, Z. X. Zhang, D. W. Fu and R. G. Xiong, *Matter*, 2020, **2**, 697–710.
34 Y. Y. Tang, P. F. Li, W. Y. Zhang, H. Y. Ye, Y. M. You and R. G. Xiong, *J. Am. Chem. Soc.*, 2017, **139**, 13903–13908.
35 P. P. Shi, Y. Y. Tang, P. F. Li, H. Y. Ye and R. G. Xiong, *J. Am. Chem. Soc.*, 2017, **139**, 1319–1324.
36 Y. Y. Tang, W. Y. Zhang, P. F. Li, H. Y. Ye, Y. M. You and R. G. Xiong, *J. Am. Chem. Soc.*, 2016, **138**, 15784–15789.
37 X. J. Song, Z. X. Zhang, X. G. Chen, H. Y. Zhang, Q. Pan, J. Yao, Y. M. You and R. G. Xiong, *J. Am. Chem. Soc.*, 2020, **142**, 9000–9006.
38 J. Ahn, E. Lee, J. Tan, W. Yang, B. Kim and J. Moon, *Mater. Horiz.*, 2017, **4**, 851–856.
39 Y. Ai, H. P. Lv, Z. X. Wang, W. Q. Liao and R. G. Xiong, *Trends Chem.*, 2021, **3**, 1088–1099.
40 X. N. Hua, W. Q. Liao, Y. Y. Tang, P. F. Li, P. P. Shi, D. W. Zhao and R. G. Xiong, *J. Am. Chem. Soc.*, 2018, **140**, 12296–12302.
41 W. Y. Zhang, Y. Y. Tang, P. F. Li, P. P. Shi, W. Q. Liao, D. W. Fu, H. Y. Ye, Y. Zhang and R. G. Xiong, *J. Am. Chem. Soc.*, 2017, **139**, 10897–10902.
42 C.-Y. Su, Y.-F. Yao, Z.-X. Zhang, Y. Wang, M. Chen, P.-Z. Huang, Y. Zhang, W.-C. Qiao and D.-W. Fu, *Chem. Sci.*, 2022, **13**, 4794–4800.
43 H. Ye, X. X. Chen, D. X. Liu, B. Q. Zhao, Y. B. Li, Y. Zeng, W. X. Zhang and X. M. Chen, *Chem. Sci.*, 2022, **13**, 14124–14131.
44 T. T. Sha, Y. A. Xiong, Q. Pan, X. G. Chen, X. J. Song, J. Yao, S. R. Miao, Z. Y. Jing, Z. J. Feng, Y. M. You and R. G. Xiong, *Adv. Mater.*, 2019, **31**, 1901843.
45 P. P. Shi, S. Q. Lu, X. J. Song, X. G. Chen, W. Q. Liao, P. F. Li, Y. Y. Tang and R. G. Xiong, *J. Am. Chem. Soc.*, 2019, **141**, 18334–18340.
46 K. Aizu, *J. Phys. Soc. Jpn.*, 1969, **27**, 387–396.
47 H. F. Ni, J. H. Lin, C. F. Wang, Q. F. Luo, P. Z. Huang, Z. X. Zhang, D. W. Fu and Y. Zhang, *Inorg. Chem. Front.*, 2023, **10**, 7231–7237.
48 S. P. Zhao, Y. Guo, J. Wang, H. Xu, Q. Qiao and R. Y. Huang, *Polyhedron*, 2020, 178.
49 Y. Hu, F. Florio, Z. Chen, W. A. Phelan, M. A. Siegler, Z. Zhou, Y. Guo, R. Hawks, J. Jiang, J. Feng, L. Zhang, B. Wang, Y. Wang, D. Gall, E. F. Palermo, Z. Lu, X. Sun, T. M. Lu, H. Zhou, Y. Ren, E. Wertz, R. Sundararaman and J. Shi, *Sci. Adv.*, 2020, **6**, eaay4213.
50 W. Zhang and R. G. Xiong, *Chem. Rev.*, 2012, **112**, 1163–1195.
51 L. Jin, F. Li and S. Zhang, *J. Am. Ceram. Soc.*, 2014, **97**, 1–27.
52 M. M. Lun, F. L. Zhou, D. W. Fu and Q. Ye, *J. Mater. Chem. C*, 2022, **10**, 11371–11378.